Solvent effects on optical properties of molecules: A combined time-dependent density functional theory/effective fragment potential approach

Soohaeng Yoo, Federico Zahariev, Sarom Sok, and Mark S. Gordon

Citation: The Journal of Chemical Physics **129**, 144112 (2008); doi: 10.1063/1.2992049
View online: http://dx.doi.org/10.1063/1.2992049
View Table of Contents: http://aip.scitation.org/toc/jcp/129/14
Published by the American Institute of Physics

Solvent effects on optical properties of molecules: A combined time-dependent density functional theory/effective fragment potential approach

Soohaeng Yoo, Federico Zahariev, Sarom Sok, and Mark S. Gordon[a)]
Department of Chemistry, Iowa State University, Ames, Iowa 50011, USA

(Received 14 July 2008; accepted 10 September 2008; published online 14 October 2008)

A quantum mechanics/molecular mechanics (QM/MM) type of scheme is employed to calculate the solvent-induced shifts of molecular electronic excitations. The effective fragment potential (EFP) method was used for the classical potential. Since EFP has a density dependent functional form, in contrast with most other MM potentials, time-dependent density functional theory (TDDFT) has been modified to combine TDDFT with EFP. This new method is then used to perform a hybrid QM/MM molecular dynamics simulation to generate a simulated spectrum of the $n \rightarrow \pi^*$ vertical excitation energy of acetone in vacuum and with 100 water molecules. The calculated water solvent effect on the vertical excitation energy exhibits a blueshift of the $n \rightarrow \pi^*$ vertical excitation energy in acetone ($\Delta\omega_1 = 0.211$ eV), which is in good agreement with the experimental blueshift. © *2008 American Institute of Physics*. [DOI: 10.1063/1.2992049]

I. INTRODUCTION

Solvent effects on the optical properties of solutes have long held the interest of chemists and continue to be the subject of much research.[1,2] Optical properties of solutes in a solvent environment are sensitive to the nature of the solvent and solute-solvent interactions including hydrogen-bonding interactions and long-range screening.[3–5] To capture solvent effects on the optical properties of solutes using theoretical methods, first principles simulations are preferred for reliability and accuracy. However, the description of a molecular system in solution can be computationally very expensive when the solvent is explicitly included. Therefore, extended condensed phase systems are often treated using approximate approaches, such as reaction field methods[6] and combined quantum mechanics/molecular mechanics (QM/MM) simulations.[7] In particular, QM/MM algorithms have successfully been applied to the calculation of absorption spectra in condensed phase systems.[8] This study combines the use of electronic structure theory (QM) for the solute with the effective fragment potential (EFP) method[9–11] to represent explicit solvent effects on the optical properties of solutes.

The original EFP (EFP1) method was developed to understand the properties of water, as well as to treat chemical reactions in an aqueous solution.[9–11] EFP1 contains three energy terms: (1) Coulomb interactions represented by a distributed multipole expansion, (2) polarization or induction interaction represented by distributed (localized orbital) dipole polarizabilities that are iterated to self-consistency, and (3) exchange repulsion, charge transfer, and other energy terms that are not taken into account in the first two energy terms (see details in Sec. II B). The first two interaction energy terms are obtained entirely from QM calculations on isolated molecules, while the last term is determined by a fitting procedure.

The time-dependent density-functional theory (TDDFT) method is used to describe electronically excited states since TDDFT frequently yields excitation energies and properties that are in good agreement with experimental values.[12–14] TDDFT has recently been reformulated to compute discrete transition energies and oscillator strengths and has been applied to a number of different atoms and molecules.[12–15] TDDFT has already been implemented by several groups of researchers and has been applied to various closed-shell[13,14,16,17] and open-shell[18] systems. TDDFT has gained widespread use in photochemistry due to its reasonable accuracy and low computational cost.

As a test of the new combined TDDFT-EFP method, aqueous solvent effects on the electronic absorption of acetone are considered since there are extensive reference data from both experiments[3,5,19] and theoretical calculations.[20–22] In carbonyl compounds, the $S_0 \rightarrow S_1$ state is primarily an $n \rightarrow \pi^*$ excitation from a carbonyl oxygen lone pair (n) [the highest occupied molecular orbital (HOMO)] to the antibonding C=O π^*-orbital [the lowest unoccupied orbital (LUMO)] (see Fig. 1). The acetone $n \rightarrow \pi^*$ state undergoes a noticeable blueshift in an aqueous environment.[3,5,19,21,23,24]

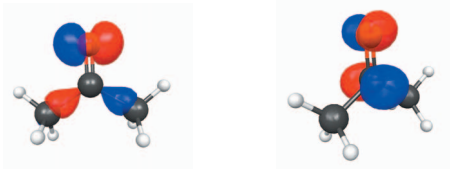

(a) HOMO (n) **(b) LUMO** (π^*)

FIG. 1. (Color) The HOMO and the LUMO of acetone. (a) The HOMO has a lone pair of the carbonyl oxygen and (b) the LUMO has an antibonding π^*-orbital on the carbonyl group.

[a)]Electronic mail: mark@si.msg.chem.iastate.edu.

In Sec. II, the TDDFT method is reviewed and the relevant equations are reformulated for the QM/EFP1 method. The simulation details are described in Sec. III. The results and discussion are presented in Sec. IV. Conclusions are given in Sec. V.

II. THEORY

The formal foundations of TDDFT have been established by Runge and Gross.[25] The Casida version[12] of the linear-response theory based on TDDFT is very convenient for excited state calculations and is the one considered here, giving only enough details to make the present paper self-contained and to document the working equations of the EFP implementation.

A. Time-dependent density-functional theory equations

The time-dependent Kohn–Sham (KS) equation

$$\left[-\frac{1}{2}\nabla^2 + v_\sigma^{\mathrm{KS}}[\rho_\alpha,\rho_\beta](\mathbf{r},t)\right]\psi_\sigma(\mathbf{r},t) = i\frac{\partial}{\partial t}\psi_\sigma(\mathbf{r},t) \tag{1}$$

can be derived, assuming the existence of a KS potential $v_\sigma^{\mathrm{KS}}[\rho_\alpha,\rho_\beta](\mathbf{r},t)$ for an independent particle system. The notation $v_\sigma^{\mathrm{KS}}[\rho_\alpha,\rho_\beta](\mathbf{r},t)$ indicates that the KS potential v_σ^{KS} has a functional dependence on both the up- and down-spin densities ρ_α and ρ_β with the definition $v_\sigma^{\mathrm{KS}}[\rho_\alpha,\rho_\beta](\mathbf{r},t) = \partial E^{\mathrm{KS}}[\rho_\alpha,\rho_\beta](\mathbf{r},t)/\partial\rho_\sigma$, where σ indicates the spin. The KS potential $v_\sigma^{\mathrm{KS}}[\rho_\alpha,\rho_\beta](\mathbf{r},t)$ may be considered to be the sum of a self-consistent field (SCF) $v_\sigma^{\mathrm{SCF}}[\rho_\alpha,\rho_\beta](\mathbf{r},t)$ and a non-SCF $v_\sigma^{\text{non-SCF}}(\mathbf{r},t)$ term, as follows:

$$v_\sigma^{\mathrm{KS}}[\rho_\alpha,\rho_\beta](\mathbf{r},t) = v_\sigma^{\text{non-SCF}}(\mathbf{r},t) + v_\sigma^{\mathrm{SCF}}[\rho_\alpha,\rho_\beta](\mathbf{r},t). \tag{2}$$

The non-SCF term has no functional dependence on the KS electron spin densities and is a sum of the Coulomb attractions between a bare nucleus A with the nuclear charge Z_A and the electrons and applied field (perturbation) $v_\sigma^{\mathrm{appl}}(\mathbf{r},t)$,

$$v_\sigma^{\text{non-SCF}}(\mathbf{r},t) = -\sum_A \frac{Z_A}{|\mathbf{r}-\mathbf{R}_A|} + v_\sigma^{\mathrm{appl}}(\mathbf{r},t), \tag{3}$$

where R_A is the position of the Ath nucleus. The applied field (perturbation) $v_\sigma^{\mathrm{appl}}(\mathbf{r},t)$ is turned on slowly in the distant past. The SCF potential $v_\sigma^{\mathrm{SCF}}[\rho_\alpha,\rho_\beta](\mathbf{r},t)$ has a functional dependence on the KS electron densities ρ_α and ρ_β,

$$v_\sigma^{\mathrm{SCF}}[\rho_\alpha,\rho_\beta](\mathbf{r},t) = v_\sigma^{H}[\rho](\mathbf{r},t) + v_\sigma^{\mathrm{xc}}[\rho_\alpha,\rho_\beta](\mathbf{r},t),$$

$$v_\sigma^{H}[\rho](\mathbf{r},t) = \frac{\delta E^H}{\delta\rho_\sigma(\mathbf{r},t)} = \int \frac{\rho(\mathbf{r}',t)}{|\mathbf{r}-\mathbf{r}'|}d\mathbf{r}', \tag{4}$$

$$v_\sigma^{\mathrm{xc}}[\rho_\alpha,\rho_\beta](\mathbf{r},t) = \frac{\delta A^{\mathrm{xc}}}{\delta\rho_\sigma(\mathbf{r},t)} \approx \frac{\delta E^{\mathrm{xc}}}{\delta\rho_{\sigma,t}(\mathbf{r})} = v_{\sigma,t}^{\mathrm{xc}}[\rho_\alpha,\rho_\beta](\mathbf{r}),$$

where $v_\sigma^H[\rho](\mathbf{r},t)$ and $v_\sigma^{\mathrm{xc}}[\rho_\alpha,\rho_\beta](\mathbf{r},t)$ are the Hartree (commonly referred to as Coulomb) and exchange-correlation potentials and E^H and E^{XC} are the Hartree and exchange-correlation energies, respectively.

The electron density ρ depends on the spin-up (α) and spin-down (β) electron densities,

$$\rho(\mathbf{r},t) = \rho_\alpha(\mathbf{r},t) + \rho_\beta(\mathbf{r},t). \tag{5}$$

The linear response based on the above formulation leads to the following non-Hermitian equation, with the excitation energies ω as the eigenvalues:

$$\begin{pmatrix}\mathbf{A} & \mathbf{B}\\ \mathbf{B} & \mathbf{A}\end{pmatrix}\begin{pmatrix}\mathbf{X}\\ \mathbf{Y}\end{pmatrix} = \omega\begin{pmatrix}1 & 0\\ 0 & -1\end{pmatrix}\begin{pmatrix}\mathbf{X}\\ \mathbf{Y}\end{pmatrix}, \tag{6}$$

where the matrices $\mathbf{A}$ and $\mathbf{B}$ are defined as

$$A_{ia\mu,jb\nu} = \delta_{ij}\delta_{ab}\delta_{\mu\nu}(\varepsilon_a - \varepsilon_i) + K_{ia\mu,jb\nu}$$

and

$$B_{ia\mu,jb\nu} = K_{ia\mu,bj\nu}.$$

Here, indices i and j are used for ground state occupied orbitals and indices a and b are used for ground state virtual orbitals. μ, ν, and σ indicate spin. ε_i is the KS energy value corresponding to the unperturbed KS orbital ψ_i of the ground state.

Now consider the coupling matrix $\mathbf{K}$,[26]

$$K_{ia\mu,jb\nu} = \frac{\partial F_{ia\mu}}{\partial P_{jb\nu}}, \tag{7}$$

where the Fock matrix $F_{ia\sigma}$ is given as

$$F_{ia\sigma} = \int \psi_{i\sigma}^*(\mathbf{r})\left(-\frac{1}{2}\nabla^2 + \sum_A \frac{-Z_A}{|\mathbf{r}-\mathbf{R}_A|} + v_\sigma^{\mathrm{SCF}}(\mathbf{r})\right)\psi_{a\sigma}(\mathbf{r})d\mathbf{r}, \tag{8}$$

and the density matrix $P_{ia\sigma}$ is related to the density $\rho_\sigma(\mathbf{r})$ by

$$\rho_\sigma(\mathbf{r}) = \sum_{i,a}\left[P_{ia\sigma}\psi_{a\sigma}^*(\mathbf{r})\psi_{i\sigma}(\mathbf{r}) + P_{ai\sigma}\psi_{a\sigma}(\mathbf{r})\psi_{i\sigma}^*(\mathbf{r})\right]. \tag{9}$$

It follows that

$$K_{ia\mu,jb\nu} = \int \psi_{i\mu}^*(\mathbf{r})\frac{\partial v_\mu^{\mathrm{SCF}}(\mathbf{r})}{\partial P_{jb\nu}}\psi_{a\mu}(\mathbf{r})d\mathbf{r}. \tag{10}$$

The Fock matrix depends on the density only through the functional dependence in $v_\sigma^{\mathrm{SCF}}[\rho_\alpha,\rho_\beta](\mathbf{r})$. (The explicit notation of this functional dependence is suppressed in all the other formulas for simplicity.) Using the definitions of $v_\sigma^{\mathrm{SCF}}(\mathbf{r})$ and density $\rho_\sigma(\mathbf{r})$ provided in Eqs. (4) and (9), together with the chain rule, the coupling matrix becomes

$$\begin{aligned}K_{ia\mu,jb\nu} &= \sum_\sigma \int\int \psi_{i\mu}^*(\mathbf{r})\left(\frac{\delta v_\mu^H(\mathbf{r})}{\delta\rho_\sigma(\mathbf{r}')}\frac{\partial\rho_\sigma(\mathbf{r}')}{\partial P_{jb\nu}} + \frac{\delta v_\mu^{\mathrm{xc}}(\mathbf{r})}{\delta\rho_\sigma(\mathbf{r}')}\frac{\partial\rho_\sigma(\mathbf{r}')}{\partial P_{jb\nu}}\right)\psi_{a\mu}(\mathbf{r})d\mathbf{r}d\mathbf{r}'\\ &= \int\int \psi_{i\mu}^*(\mathbf{r})\psi_{a\mu}(\mathbf{r})\frac{1}{|\mathbf{r}-\mathbf{r}'|}\psi_{j\nu}(\mathbf{r}')\psi_{b\nu}^*(\mathbf{r}')d\mathbf{r}d\mathbf{r}'\\ &\quad + \int\int \psi_{i\mu}^*(\mathbf{r})\psi_{a\mu}(\mathbf{r})\frac{\delta v_\mu^{\mathrm{xc}}}{\delta\rho_\nu(\mathbf{r}')}\psi_{j\nu}(\mathbf{r}')\psi_{b\nu}^*(\mathbf{r}')d\mathbf{r}d\mathbf{r}'.\end{aligned} \tag{11}$$

Starting from a restricted KS calculation for the ground state ($\rho_\alpha = \rho_\beta$), one can use the following unitary transformation:

$$u_{ia}^{s} = \frac{1}{\sqrt{2}}(P_{ia\alpha} + P_{ia\beta}),$$

$$u_{ia}^{t} = \frac{1}{\sqrt{2}}(P_{ia\alpha} - P_{ia\beta}), \tag{12}$$

to distinguish between singlet ($\rho_\alpha = \rho_\beta$) and triplet excitations (breaking $\rho_\alpha = \rho_\beta$).[13] u^s is used for the singlet excitation and u^t for the triplet excitation.

B. Solvent effects by the effective fragment potential method

In this work, the solvent is treated with EFP1.[9,11] To include solvent effects within the time-dependent KS formalism, the solute-solvent interaction term $v^{\mathrm{EFP1}}(\mathbf{r},t)$ is added into the KS potential $v_\sigma^{\mathrm{KS}}[\rho_\alpha,\rho_\beta](\mathbf{r},t)$. To demonstrate that the EFP1 potential can be defined as a density dependent functional, consider the interaction energy between an EFP1 and a KS electron. The EFP1 interaction energy with the KS electron density $\rho(\mathbf{r})$ consists of Coulomb interaction, polarization, and a remainder contribution that are discussed below,

$$E^{\mathrm{EFP1}} = \sum_{\eta}\left[\sum_{k=1}^{K} E_k^{\mathrm{elec}}(\eta) + \sum_{l=1}^{L} E_l^{\mathrm{pol}}(\eta) + \sum_{m=1}^{M} E_m^{\mathrm{rem}}(\eta)\right], \tag{13}$$

where η sums over the solvent molecules. For the ηth solvent molecule, these contributions are expanded over a number (K, L, and M) of expansion points.

For water molecules, the expansion of the Coulomb interaction is carried out through octupole moments at $K=5$ points (nuclear centers and bond midpoints). The expression for the Coulomb interaction of EFP1 with the electron density $\rho(\mathbf{r})$ of the QM part is

$$E_k^{\mathrm{elec}}(\eta) = E_k^{\mathrm{monopole}} + E_k^{\mathrm{dipole}} + E_k^{\mathrm{quadrupole}} + E_k^{\mathrm{octupole}},$$

$$E_k^{\mathrm{monopole}} = \int [q_k^{\mathrm{nuc}} + q_k^{\mathrm{ele}}\Phi_k^{\mathrm{pen}}(R_k)]\frac{-\rho(\mathbf{r})}{R_k}d\mathbf{r},$$

$$E_k^{\mathrm{dipole}} = \int \sum_{p}^{x,y,z} \mu_p^k F_p(\mathbf{R}_k)\Phi_k^{\mathrm{pen}}(R_k)\frac{-\rho(\mathbf{r})}{R_k^3}d\mathbf{r},$$

$$E_k^{\mathrm{quadrupole}} = \int \sum_{p}^{x,y,z}\sum_{q}^{x,y,z} \Theta_{pq}^k F_{pq}(\mathbf{R}_k)\Phi_k^{\mathrm{pen}}(R_k)\frac{-\rho(\mathbf{r})}{3R_k^5}d\mathbf{r}, \tag{14}$$

$$E_k^{\mathrm{octupole}} = \int \sum_{p}^{x,y,z}\sum_{q}^{x,y,z}\sum_{r}^{x,y,z} \Omega_{pqr}^k F_{pqr}(\mathbf{R}_k)\Phi_k^{\mathrm{pen}}(R_k)\frac{-\rho(\mathbf{r})}{5R_k^7}d\mathbf{r},$$

$$\Phi_k^{\mathrm{pen}}(R_k) = 1 - \beta_k \exp(-\alpha_k R_k^2),$$

where the subscript k refers to a multipole center in the molecule. μ_p is a first-order dipole tensor, Θ_{pq} is a second-order quadrupole tensor, and Ω_{pqr} is a third-order octupole tensor. F_p, F_{pq}, and F_{pqr} are (respectively) the solute electric field, field gradient (first derivative), and field Hessian (second derivative) of the electron density $\rho(\mathbf{r})$. $\Phi_k^{\mathrm{pen}}(R_k)$ is a distance dependent screening function that is employed to account for overlapping charge densities.[27] α_k and β_k in $\Phi_k^{\mathrm{pen}}(R_k)$ are screening parameters,[27] and R_k is the distance between the multipole center k and the electron density $\rho(\mathbf{r})$.

The second EFP1 energy contribution is the polarization, or induction, energy that is expressed in terms of localized molecular orbital (LMO) polarizability tensors. For water, there are five LMOs, so $L=5$ in Eq. (13): O inner shell, two O lone pairs, and two O–H bonds. The polarization energy is iterated to self-consistency,

$$E_l^{\mathrm{pol}}(\eta) = -\frac{1}{2}\mu_l \cdot \left[\int -\rho(\mathbf{r})\frac{\mathbf{r}_l - \mathbf{r}}{R_l^3}d\mathbf{r}\right]. \tag{15}$$

Here, the subscript l refers to a polarizability point. $\boldsymbol{\mu}_l$ is the induced dipole moment at site l. Assuming that the induced dipole moment is a linear function of the applied field,

$$\mu_l = \tilde{\alpha}\mathbf{F}_l,$$

$$\mathbf{F}_l = \mathbf{F}_l^{\mathrm{elec}} + \cdots, \tag{16}$$

$$\mathbf{F}_l^{\mathrm{elec}} = -\int \rho(\mathbf{r})\frac{\mathbf{r}_l - \mathbf{r}}{R_l^3}d\mathbf{r},$$

where $\tilde{\alpha}$ is the polarizability tensor at point l and $\mathbf{F}_l$ is the applied field vector at point l. The total electric field $\mathbf{F}_l^{\mathrm{elec}}$ is the contribution to the field from the KS electrons and has a density dependent functional form.

The last EFP1 energy term in Eq. (13) is a remainder (rem) term that includes those components of the interaction energy that are not accounted for by the Coulomb and induction terms. If EFP1 is based on Hartree–Fock (EFP1/HF), E^{rem} contains the exchange repulsion+charge transfer, as noted by Kitaura and Morokuma.[28] If EFP1 is based on density functional theory (EFP1/DFT),[11] the remainder term also includes some dynamic correlation corrections. In general,

$$E_m^{\mathrm{rem}}(\eta) = \int \sum_{j}[\beta_{m,j}\exp(-\alpha_{m,j}R_m^2)]\rho(\mathbf{r})d\mathbf{r}, \tag{17}$$

where m refers to a fragment center for the exchange repulsion potential. α and β are parameters that are fitted to either the HF (EFP1/HF) or the DFT (EFP1/DFT) water dimer potential energy surface.

With the definition of the EFP1 potential,

$$v_\sigma^{\mathrm{EFP1}}(\mathbf{r}) = \delta E^{\mathrm{EFP1}}/\delta\rho_\sigma(\mathbf{r}),$$

the induction part of the potential,

$$v_\sigma^{\mathrm{pol}}(\mathbf{r}) = \delta E^{\mathrm{pol}}/\delta\rho_\sigma(\mathbf{r}),$$

can be expressed in terms of the density,

$$v_\sigma^{\mathrm{pol}}(\eta,\mathbf{r}) = \sum_l \frac{\delta E_l^{\mathrm{pol}}(\eta)}{\delta\rho_\sigma(\mathbf{r})} = \frac{1}{2}\sum_l \left(\mu_l \cdot \left[\frac{\mathbf{r}_l - \mathbf{r}}{R_l^3} \right] + \frac{\delta\mu_l}{\delta\rho_\sigma(\mathbf{r})} \cdot \int \rho(\mathbf{r}') \frac{\mathbf{r}_l - \mathbf{r}'}{R_l'^3} d\mathbf{r}' \right). \quad (18)$$

Since the induced dipole moment $\boldsymbol{\mu}_l$ is a density dependent functional, the polarization potential $v_\sigma^{\mathrm{pol}}[\rho]$ becomes a density dependent functional. This polarization potential is added to the SCF potential $v_\sigma^{\mathrm{SCF}}[\rho_\alpha,\rho_\beta](\mathbf{r},t)$ as

$$v_\sigma^{\mathrm{SCF}}[\rho_\alpha,\rho_\beta](\mathbf{r},t) = v_\sigma^{H}[\rho](\mathbf{r},t) + v_\sigma^{\mathrm{xc}}[\rho_\alpha,\rho_\beta](\mathbf{r},t) + v_\sigma^{\mathrm{pol}}[\rho](\mathbf{r},t). \quad (19)$$

The other two EFP1 terms, the Coulomb and exchange repulsion/charge transfer interactions, are added to the non-SCF potential $v_\sigma^{\text{non-SCF}}(\mathbf{r},t)$.

C. Linear-response TDDFT/EFP1

Since only the induced polarization part of EFP1 depends on the density change [see Eqs. (18) and (19)], this term will be the only contributor to the modified coupling matrix **K** of the linear-response TDDFT eigenvalue equation,

$$\begin{aligned} K_{ia\mu,jb\nu} &= \sum_\sigma \int\int \psi_{i\mu}^*(\mathbf{r}) \left(\frac{\delta v_\mu^H(\mathbf{r})}{\delta\rho_\sigma(\mathbf{r}')} \frac{\partial\rho_\sigma(\mathbf{r}')}{\partial P_{jb\nu}} + \frac{\delta v_\mu^{\mathrm{xc}}(\mathbf{r})}{\delta\rho_\sigma(\mathbf{r}')} \frac{\partial\rho_\sigma(\mathbf{r}')}{\partial P_{jb\nu}} + \frac{\delta v_\mu^{\mathrm{pol}}(\mathbf{r})}{\delta\rho_\sigma(\mathbf{r}')} \frac{\partial\rho_\sigma(\mathbf{r}')}{\partial P_{jb\nu}} \right) \psi_{a\mu}(\mathbf{r}) d\mathbf{r} d\mathbf{r}' \\ &= \int\int \psi_{i\mu}^*(\mathbf{r}) \psi_{a\mu}(\mathbf{r}) \frac{1}{|\mathbf{r}-\mathbf{r}'|} \psi_{j\nu}(\mathbf{r}') \psi_{b\nu}^*(\mathbf{r}') d\mathbf{r} d\mathbf{r}' \\ &\quad + \int\int \psi_{i\mu}^*(\mathbf{r}) \psi_{a\mu}(\mathbf{r}) \frac{\delta v_\mu^{\mathrm{xc}}}{\delta\rho_\nu(\mathbf{r}')} \psi_{j\nu}(\mathbf{r}') \psi_{b\nu}^*(\mathbf{r}') d\mathbf{r} d\mathbf{r}' \\ &\quad + \int\int \psi_{i\mu}^*(\mathbf{r}) \psi_{a\mu}(\mathbf{r}) \frac{\delta v_\mu^{\mathrm{pol}}}{\delta\rho_\nu(\mathbf{r}')} \psi_{j\nu}(\mathbf{r}') \psi_{b\nu}^*(\mathbf{r}') d\mathbf{r} d\mathbf{r}'. \end{aligned} \quad (20)$$

Since the induced dipole moment depends on the density change, the last term $\delta v_\mu^{\mathrm{pol}}[\rho](\mathbf{r})/\delta\rho_\nu(\mathbf{r}')$ in Eq. (20) can be calculated using Eq. (18). This term is given by

$$\frac{\delta v_\mu^{\mathrm{pol}}[\rho](\mathbf{r})}{\delta\rho_\nu(\mathbf{r}')} = -\frac{1}{2}\sum_\eta \sum_l \left(\left[\tilde{\alpha}_l \frac{\mathbf{r}_l - \mathbf{r}}{R_l^3} \right] \cdot \frac{\mathbf{r}_l - \mathbf{r}'}{R_l'^3} + \left[\tilde{\alpha}_l \frac{\mathbf{r}_l - \mathbf{r}'}{R_l'^3} \right] \cdot \frac{\mathbf{r}_l - \mathbf{r}}{R_l^3} \right) \frac{\delta\rho(\mathbf{r})}{\delta\rho_\nu(\mathbf{r}')}. \quad (21)$$

Note that

$$\frac{\delta\rho(\mathbf{r})}{\delta\rho_\nu(\mathbf{r}')} = \delta(\mathbf{r}-\mathbf{r}'), \quad (22)$$

where $\delta(\mathbf{r}-\mathbf{r}')$ is a Dirac delta function. $\tilde{\alpha}_\ell$ is the polarizability tensor at point l.

Inserting Eqs. (21) and (22) into the last (explicit solvent) term in Eq. (20) gives the following:

$$\begin{aligned} &-\frac{1}{2}\sum_\eta \sum_l \left(\int \psi_{i\mu}(\mathbf{r}) \left[\tilde{\alpha} \frac{\mathbf{r}_l - \mathbf{r}}{R_l^3} \right] \psi_{a\mu}(\mathbf{r}) d\mathbf{r} \cdot \int \psi_{j\nu}(\mathbf{r}) \left[\frac{\mathbf{r}_l - \mathbf{r}}{R_l^3} \right] \psi_{b\nu}(\mathbf{r}) d\mathbf{r} \right. \\ &\left. + \int \psi_{i\mu}(\mathbf{r}) \left[\frac{\mathbf{r}_l - \mathbf{r}}{R_l^3} \right] \psi_{a\mu}(\mathbf{r}) d\mathbf{r} \cdot \int \psi_{j\nu}(\mathbf{r}) \left[\tilde{\alpha} \frac{\mathbf{r}_l - \mathbf{r}}{R_l^3} \right] \psi_{b\nu}(\mathbf{r}) d\mathbf{r} \right). \end{aligned} \quad (23)$$

GAMESS (Ref. 29) uses a modified Davidson algorithm for determining the lowest few eigenvalues (or excitation energies) and eigenvectors for a large non-Hermitian matrix.[17] For a spin-restricted KS calculation, which implies $\psi_{i\alpha}(\mathbf{r}) = \psi_{i\beta}(\mathbf{r})$ (and hence $\rho_\alpha = \rho_\beta$), the matrices **A** and **B** in Eq. (16) for singlet excitations include the solvent contribution. For triplet excitations, the solvent contribution in Eq. (23) is eliminated after the unitary transformation to u_{ia}^t of Eq. (12) for the same reason that the Hartree (Coulomb) component is eliminated in conventional TDDFT due to the spin independence of Eq. (23).[13] The EFP1 solvent molecules affect the UV spectrum, as computed within the combined TDDFT/EFP1 scheme presented above, in two ways. There is a direct EFP1 contribution due to the $v_\sigma^{\mathrm{pol}}(\eta,\mathbf{r})$ component of the modified coupling matrix K given in Eq. (23), as well as an indirect EFP1 contribution because the electronic spin density is affected by the EFP1 solvent, which in turn affects the regular components of the coupling matrix K, the exchange-correlation component in particular. While the singlet excitations include both the direct and indirect EFP1 contributions, the triplet excitations are affected only indirectly by the EFP1 solvent. Nevertheless, the net result differs from the gas-phase calculation. Note that in the present implementation, only the static electronic response is included in the TDDFT calculation of the solvated molecule. In subsequent developments, the full responses of the solvent molecules at the excitation frequency will be incorporated as well.

III. COMPUTATIONAL APPROACH

The optical properties of solutes are sensitive to their molecular structures.[2] Furthermore, their optical properties in solvent environments are sensitive to the nature of the solvent and solute-solvent interactions,[3–5] which can be quite complex, involving hydrogen-bonding and long-range screening. To capture the effects of solvents on the optical properties of solutes, the DFT based EFP1 model (EFP1/DFT)[11] was employed. The EFP1/DFT solvent model was developed based on the B3LYP functional[30] and the Dunning–Hay (DH) basis set with d polarization functions on oxygen and p polarization functions on hydrogen atoms.[11] For consistency, the QM potential energy surfaces in the present work were obtained with the B3LYP functional and the DH(d,p) basis set.[31]

Born–Oppenheimer *ab initio* molecular dynamics (MD) was employed to propagate the nuclei for the QM region of the solute with explicit solute-solvent molecular interactions. An isolated system consists of 100 EFP1/DFT water mol-

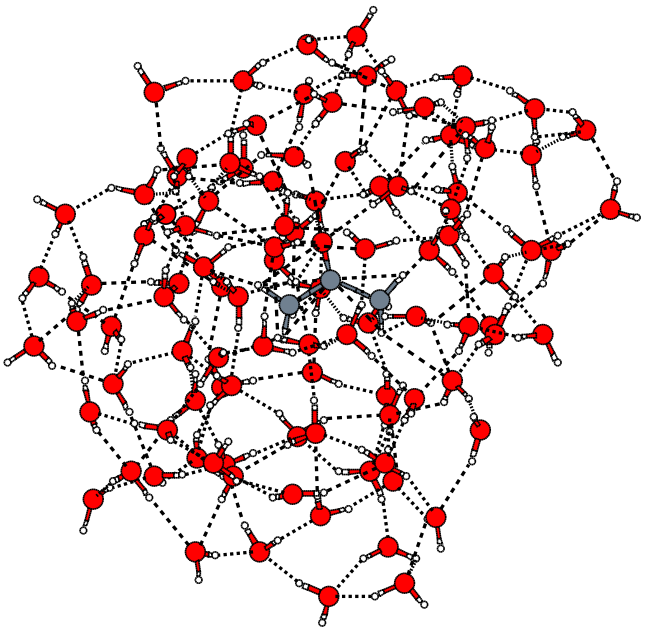

FIG. 2. (Color online) Snapshot of acetone with 100 EFP1 during the MD simulation of QM/MM.

ecules and one acetone molecule (see Fig. 2). 100 EFP1/DFT water molecules were within 10 Å from the acetone molecule. Here the acetone molecule belongs to the QM region, and the EFP1/DFT water molecules belong to the MM region. Potential energy calculations among EFP1/DFT water molecules were treated with a simple switching function to shift the pairwise potential function to zero from 7 to 9 Å smoothly. To mimic the isolated system, in which the long-range interactions between water molecules in a box and those in its replicas were not allowed, a large box length of 100 Å was chosen. The Nose–Hoover chain method[32] was employed to perform the canonical ensemble (*NVT*) simulation with a temperature of 300 K. The time step was chosen to be $dt=1.0$ fs. The data reported here have been obtained from equilibrated trajectories of 3–6 ps length during which snapshots were gathered every 10 fs. A short MD simulation was used to avoid the evaporation of water. To calculate the vertical excitation energy at each snapshot structure via TD-DFT, the default grid (96^*12^*24 points per atom) was used in all ground state DFT calculations. A smaller grid (24^*8^*16 points per atom) was used for the excitation energy calculations. This reproduces the full grid excitation energies to within 0.001 eV. All calculations were done using the electronic structure code GAMESS.[29]

IV. RESULTS AND DISCUSSION

In acetone, the $S_0 \rightarrow S_1$ excitation is an $n \rightarrow \pi^*$ excitation from a lone pair of the carbonyl oxygen (HOMO) [Fig. 1(a)] to the antibonding π^*-orbital of the CO double bond (LUMO) [Fig. 1(b)]. For the optimized ground state structure of acetone in vacuum, TDDFT B3LYP/DH(d,p) calculations yield a vertical excitation energy of 4.417 eV for the $S_0 \rightarrow S_1$ transition, in good agreement with the experimental

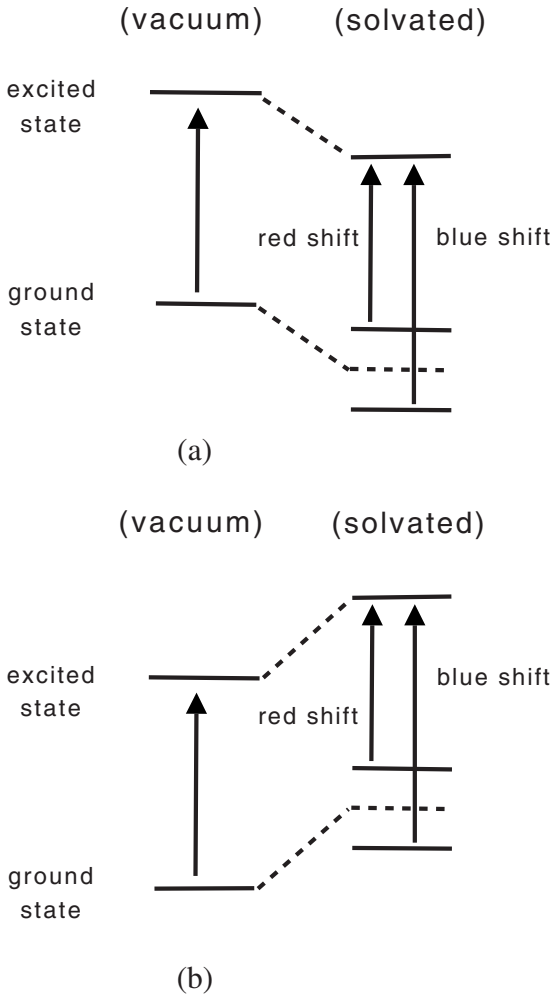

FIG. 3. Schematic illustration of energy level diagrams of the solute for understanding how its electronic states are changed due to the solvent effect. The vertical excitation energies required for transitions from ground to excited states are indicated with arrows. Two possible solvent interactions with the solute are considered: (a) The solvent stabilizes the solute's ground and excited states and (b) the solvent destabilizes the solute's ground and excited states. The dashed lines indicate the situation in which the excited state has the same electron distribution as the ground state.

value of 4.48 eV.[5,19] The CO bond distance of optimized acetone in vacuum is 1.221 Å, again in good agreement with the experimental value of 1.213 Å.

To understand the effect of the solvent on the vertical excitation energy, it suffices to assess the impact of solute-solvent interactions on the electronic ground state and on the first excited state, as shown in Fig. 3. The total excited state energy is the sum of the ground state energy and the vertical excitation energy. Since the electron density distribution of the excited state is not the same as that of the ground state, it is expected that the electronic interaction of the excited state with the solvent will differ from that of the ground state. This difference in the electronic interaction with the solvent gives the solvent-induced redshift (or blueshift). To obtain a *qualitative* interpretation of the calculated solvent-induced shift in the excitation energy, one can examine the changes in the energies of the solute HOMO and LUMO due to the solvent. Figure 3 illustrates two possible solvent-induced shifts on the solute HOMO and LUMO: (a) if the HOMO is more (or less)

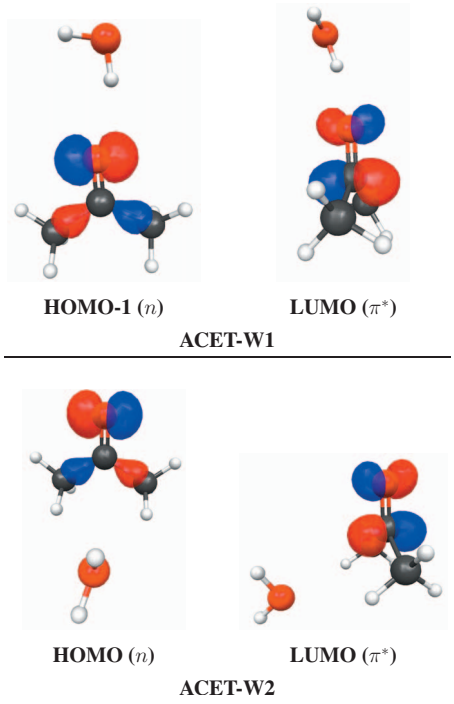

FIG. 4. (Color) Two possible optimized water and acetone dimers.

stabilized than the LUMO in the solvated system, one can expect a blueshift (or redshift) in the vertical excitation energy when compared to the gas-phase system; (b) if both the HOMO and the LUMO are destabilized, and if the HOMO is more (or less) destabilized than the LUMO in the solvated system, there will be a solvent-induced redshift (or blueshift) in the vertical excitation energy.

Two acetone-water dimers are considered, as shown in Fig. 4. Structure ACET-W1 has the carbonyl group of the acetone involved in hydrogen bonds with the water molecule, while structure ACET-W2 has no hydrogen bonds. The vertical excitation energy and the HOMO and LUMO orbital energies are provided in Table I for these structures. Upon complexation with a water molecule, ACET-W1 exhibits a larger blueshift in the vertical excitation energy than does ACET-W2. Note that the HOMO and LUMO orbital energies are shifted in both ACET-W1 and ACET-W2 relative to those of acetone in vacuum. The hydrogen bond between the CO group and water stabilizes both the HOMO and LUMO [see Fig. 3(a)] in ACET-W1 since the hydrogen atom of the water molecule has a partial positive charge that produces an attractive interaction with the electronic density

TABLE I. The CO distance (R_{CO}) for acetone and acetone-water dimer in vacuum is given in Å; the vertical excitation energy (ω_1) and the HOMO and LUMO orbital energies are given in eV.

	R_{CO}	$\omega_1(n\rightarrow\pi^*)$	HOMO	LUMO
Experiment (gas)		4.480		
Acetone	1.221	4.417	−6.737	−0.386
ACET-W1	1.223	4.490	−7.310	−0.904
ACET-W2	1.222	4.446	−6.363	0.011
ACET-EFP1	1.223	4.473	−7.204	−0.810
ACET-EFP2	1.222	4.448	−6.386	−0.010

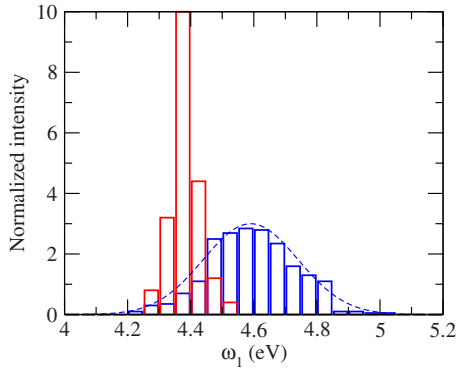

FIG. 5. (Color online) The simulated spectrum for the $n\rightarrow\pi^*$ vertical excitation energy of the acetone (here, the left-most line is for the acetone in vacuum and the right-most line is for the solvated acetone).

on the CO group. For ACET-W2, the oxygen atom (partial negative charge) of the water molecules has a repulsive interaction with both the HOMO and LUMO. Both the HOMO and LUMO are destabilized slightly due to the repulsive interaction of the CO group with water [see Fig. 3(b)]. Since the HOMO is a nonbonding orbital located mainly at the carbonyl oxygen atom, the oxygen electron density is larger than that on the carbonyl carbon atom. In the LUMO, on the other hand, the oxygen electronic density is smaller than that on the carbon atom. These different electron distributions in the HOMO and the LUMO are expected to interact differently with water. For example, the HOMO of ACET-W1 is stabilized by 0.573 eV compared to acetone in vacuum, while the LUMO is stabilized by 0.515 eV. Since ACET-W2 has no hydrogen bonds, its LUMO is destabilized by 0.397 eV, while the HOMO is destabilized by 0.374 eV.

To assess the accuracy of the QM/EFP TDDFT approach, the water molecules in the foregoing discussion were replaced with EFP1/DFT waters, and the calculations were repeated. As shown in Table I, the TDDFT/EFP1 shifts in vertical excitation energies reproduce those using the fully QM system to within ~0.02 eV. The orbital energy changes of the acetone HOMO and the LUMO are also consistent with those obtained using the all-QM calculation. This suggests that the combined QM/EFP1 method should be reliable for more extensive fluid simulations to examine the solvent effects on the optical properties of acetone.

MD simulations were performed at 300 K to generate a simulated spectrum of the $n\rightarrow\pi^*$ absorption energy of acetone in vacuum and with 100 water molecules. The resulting predicted spectrum is shown in Fig. 5, where the left-most line is for acetone in vacuum and the right-most line is for solvated acetone. The average values for the $n\rightarrow\pi^*$ ex-

TABLE II. The average CO distance (R_{CO}) as well as the average values of the vertical excitation (ω_1), HOMO, and LUMO energies, which are obtained from the equilibrated MD trajectories (see Fig. 5). Energies are given in eV and distances in Å.

	R_{CO}	$\omega_1(n\rightarrow\pi^*)$	HOMO	LUMO
Acetone in gas	1.222	4.382	−6.744	−0.443
Acetone in solvent	1.233	4.593	−7.124	−0.634
Δ	0.011	0.211	−0.380	−0.191

citation energy are given in Table II. The average excitation energy in vacuum (4.382 eV) is slightly redshifted in comparison to the vertical excitation energy (4.417 eV) of the optimized structure in vacuum. During MD simulations at 300 K, the geometry of acetone in vacuum fluctuates. The fluctuating geometries of acetone at 300 K are not the same as the optimized geometry. To understand the redshifted vertical excitation energy, the scheme in Fig. 3 can be applied to acetone in vacuum. Since the $n \rightarrow \pi^*$ absorption occurs mostly on the carbonyl group, consider the CO bond distance. The average CO bond distance (1.222 Å) of the isolated acetone geometries at 300 K is slightly elongated in comparison with that (1.221 Å) of the optimized geometry. Due to the slightly elongated CO bond distance, both average HOMO and LUMO orbital energies at 300 K are lowered in energy, as shown in Fig. 3(a). The LUMO orbital energy is lowered more than the HOMO orbital energy. This occurs because the LUMO, which possesses a CO nodal plane, is stabilized with increasing CO bond distance, while the HOMO, a nonbonding orbital located mainly at the oxygen atom, is much less affected by this geometrical fluctuation. The present calculations are consistent with this rationale.[20,21,23]

The vertical excitation energy in the presence of the solvent exhibits a slightly broader Gaussian type distribution (broken line in Fig. 5) than that in the gas phase, and the average vertical excitation energy of 4.593 eV of the solvated acetone is blueshifted by $\Delta\omega_1 = 0.211$ eV (see Table II). The experimental blueshift of $\Delta\omega_1 = 0.19-0.21$ eV is thus well reproduced. The hydrogen bonds of the acetone carbonyl group with water stabilize the HOMO more than the LUMO (see Table II), as discussed above. The main contribution to the blueshift excitation is the lowering of the HOMO orbital energy.

V. CONCLUSIONS

A combined QM/MM approach, in which QM is represented by the DFT or TDDFT and MM is represented by the EFP, has been employed to calculate the optical properties of solvated acetone. Since the EFP model includes a polarization contribution that is density dependent, the TDDFT equations were reformulated to incorporate this effect. Using these modified TDDFT equations, it was demonstrated that the QM/EFP method accurately reproduces the all-QM vertical excitation energy for a 1:1 acetone:water complex. The solvent-induced QM/EFP vertical excitation energy in the presence of water was investigated using MD simulation in the presence of 100 EFP water molecules. The experimental blueshift is well reproduced by the method. To interpret the observed solvent effect, the acetone carbonyl group was shown to influence the $S_0 \rightarrow S_1$ excitation. Since the HOMO has higher electron density on the oxygen atom, while the LUMO favors the carbon atom, the hydrogen bonds between the carbonyl group and the water stabilize the HOMO slightly more than the LUMO. This leads to the observed blueshift.

ACKNOWLEDGMENTS

This work was supported by a SBIR grant from the Air Force.

[1] A. M. Moran and A. M. Kelley, J. Chem. Phys. **115**, 912 (2001); Z. R. Grabowski and K. Rotkiewicz, Chem. Rev. (Washington, D.C.) **103**, 3899 (2003).
[2] M. Yu Balakina and E. N. Sergey, Int. J. Quantum Chem. **106**, 2245 (2006).
[3] N. S. Bayliss and E. G. McRae, J. Phys. Chem. **58**, 1006 (1954).
[4] N. S. Bayliss and E. G. McRae, J. Phys. Chem. **58**, 1002 (1954).
[5] N. S. Bayliss and G. Will-Johnson, Spectrochim. Acta, Part A **24**, 551 (1968).
[6] D. M. Chipman, Theor. Chem. Acc. **107**, 80 (2002); D. M. Chipman and M. Dupuis, *ibid.* **107**, 90 (2002).
[7] A. Warshel and M. Levitt, J. Mol. Biol. **103**, 227 (1976); U. C. Singh and P. A. Kollman, J. Comput. Chem. **7**, 718 (1986); M. J. Field, P. A. Bash, and M. Karplus, *ibid.* **11**, 700 (1990).
[8] V. Luzhkov and A. Warshel, J. Am. Chem. Soc. **113**, 4491 (1991); A. Broo, G. Pearl, and M. C. Zerner, J. Phys. Chem. A **101**, 2478 (1997); S. Hayashi, E. Tajkhorshid, and K. Schulten, Biophys. J. **83**, 1281 (2002); J. Kongsted, A. Osted, K. V. Mikkelsen, and O. Christiansen, J. Chem. Phys. **118**, 1620 (2003).
[9] P. N. Day, J. H. Jensen, M. S. Gordon, S. P. Webb, W. J. Stevens, M. Krauss, and D. Garmer, J. Chem. Phys. **105**, 1968 (1996).
[10] J. H. Jensen and M. S. Gordon, J. Chem. Phys. **108**, 4772 (1998).
[11] I. Adamovic, M. A. Freitag, and M. S. Gordon, J. Chem. Phys. **118**, 6725 (2003).
[12] M. E. Casida, *Recent Advances in Density Functional Methods* (World Scientific, Singapore, 1995); M. E. Casida, *Recent Developments and Applications of Modern Density Functional Theory, Theoretical and Computational Chemistry* (Elsevier, Amsterdam, 1996).
[13] R. Bauernschmitt and R. Ahlrichs, Chem. Phys. Lett. **256**, 454 (1996).
[14] R. Bauernschmitt, M. H. Häser, O. Treutler, and R. Ahlrichs, Chem. Phys. Lett. **264**, 573 (1997).
[15] M. E. Casida and T. A. Wesolowski, Int. J. Quantum Chem. **96**, 577 (2004); J. Neugebauer, M. J. Louwerse, E. J. Baerends, and T. A. Wesolowski, J. Chem. Phys. **122**, 094115 (2005).
[16] C. Jamorski, M. E. Casida, and D. R. Salahub, J. Chem. Phys. **104**, 5134 (1996); K. B. Wiberg, R. E. Stratmann, and M. J. Frisch, Chem. Phys. Lett. **297**, 60 (1998); M. E. Casida, C. Jamorski, K. C. Casida, and D. R. Salahub, J. Chem. Phys. **108**, 4439 (1998); D. J. Tozer and N. C. Handy, *ibid.* **109**, 10180 (1998).
[17] R. E. Stratmann, G. E. Scuseria, and M. J. Frisch, J. Chem. Phys. **109**, 8218 (1998).
[18] S. Hirata and M. Head-Gordon, Chem. Phys. Lett. **302**, 375 (1999).
[19] W. P. Hayes and C. J. Timmons, Spectrochim. Acta **21**, 529 (1965).
[20] U. F. Röhrig, I. Frank, J. Hutter, A. Laio, J. VandeVondele, and U. Rothlisberger, ChemPhysChem **4**, 1177 (2003).
[21] K. Aidas, J. Kongsted, A. Osted, K. V. Mikkelsen, and O. Christiansen, J. Phys. Chem. A **109**, 8001 (2005).
[22] M. Sulpizi, U. F. Rohrig, J. Hutter, and U. Rothlisberger, Int. J. Quantum Chem. **101**, 671 (2005).
[23] K. Coutinho, N. Saavedra, and S. Canuto, J. Mol. Struct.: THEOCHEM **466**, 69 (1999).
[24] K. Naka, A. Morita, and S. Kato, J. Chem. Phys. **110**, 3484 (1999).
[25] E. Runge and E. K. U. Gross, Phys. Rev. Lett. **52**, 997 (1984); E. K. U. Gross and W. Kohn, Adv. Quantum Chem. **21**, 255 (1990); R. van Leeuwen, Int. J. Mod. Phys. B **15**, 1969 (2001).
[26] S. Hirata and M. Head-Gordon, Chem. Phys. Lett. **314**, 291 (1999).
[27] L. Slipchenko and M. S. Gordon, J. Comput. Chem. **28**, 276 (2007).
[28] K. Kitaura and K. Morokuma, Int. J. Quantum Chem. **10**, 325 (1976).
[29] M. W. Schmidt, K. K. Baldridge, J. A. Boatz, S. T. Elbert, M. S. Gordon, J. H. Jensen, S. Koseki, N. Matsunaga, K. A. Nguyen, S. J. Su, T. L. Windus, M. Dupuis, and J. A. Montgomery, J. Comput. Chem. **14**, 1347 (1993).

[30] A. D. Becke, Phys. Rev. A **38**, 3098 (1988); C. Lee, W. Yang, and R. G. Parr, Phys. Rev. B **37**, 785 (1988).
[31] T. H. Dunning and P. J. Hay, *Methods of Electronic Structure Theory* (Plenum, New York, 1977).
[32] G. J. Martyna, M. E. Tuckerman, D. J. Tobias, and M. L. Klein, Mol. Phys. **87**, 1117 (1996); D. Frenkel and B. Smit, *Understanding Molecular Simulation from Algorithms to Applications*, 2nd ed. (Academic, San Diego, 2002).